Exciton-migration and three-pulse femtosecond optical spectroscopies of photosynthetic antenna complexes

Wei Min Zhang, Torsten Meier, Vladimir Chernyak, and Shaul Mukamel
*Department of Chemistry and Rochester Theory Center for Optical Science and Engineering,
University of Rochester, P.O. Box RC 270216, Rochester, New York 14627-0216*

A theory for four-wave-mixing signals from molecular aggregates, which includes effects of two-exciton states, static disorder, and coupling to a phonon bath with an arbitrary spectral density, is developed. The third-order polarization is rigorously partitioned into a coherent and a sequential contribution. The latter is given by a sum of an exciton-hopping and a ground state (bleaching) terms, both expressed using the doorway-window representation. Applications are made to photon-echo and pump-probe spectroscopies of the B850 system of the LH2 antenna in purple bacteria. © *1998 American Institute of Physics.* [S0021-9606(98)02913-4]

I. INTRODUCTION

Biological antenna complexes have recently become an object of extensive studies using a variety of ultrafast non-linear spectroscopic techniques.[1–3] Coherent and incoherent exciton dynamics in light harvesting complexes[1,2] has been probed by various time-domain optical measurements. These include fluorescence depolarization,[4,5] hole burning,[6–9] pump-probe,[10–13] and photon echoes.[14–16] The interpretation of these experiments requires a theory which incorporates exciton-exciton interactions, strong exciton-phonon coupling, and static disorder.

Theories of nonlinear optical response in molecular aggregates are usually based on the Frenkel exciton Hamiltonian[17,18] which describes an aggregate made out of two- or three-level molecules. These theories can be classified according to the level of reduction with respect to nuclear (phonon) degrees of freedom.[19] At the simplest level, the coupling to nuclei is incorporated via relaxation superoperators calculated perturbatively in exciton-phonon coupling. Such theories apply for weak exciton-phonon coupling and do not take the detailed form of nuclear spectral densities into account. The pump-probe signal, the frequency resolved fluorescence, and the superradiance have been analyzed recently using this approach.[20(a)] These studies focused on the long-time limit of the signals and did not calculate the evolution of exciton populations. Strong exciton-phonon coupling may lead to the formation of polarons (excitons dressed by a phonon cloud). In Ref. 20(b) the cooperative spontaneous emission (superradiance) of the LH2 antenna has been calculated by incorporating polaron effects using different Ansätze for the polaron wave functions. Localization of the exciton density matrix due to polaron formation was found to strongly influence the radiative decay. An alternative approach for incorporating strong exciton-phonon coupling was developed in Ref. 21(a): The Hamiltonian is first transformed to the exciton basis. The exciton-phonon coupling enters both through the diagonal and the off-diagonal elements of the Hamiltonian in this basis. The diagonal coupling represented by arbitrary spectral densities was included

exactly, whereas the phonon-dependence of the off-diagonal coupling (which is responsible for exciton hopping) has been neglected. This approximation may be used in the calculation of two-pulse four-wave-mixing signals which are not sensitive to exciton migration.

In this paper we extend the theory of Ref. 21(a) to include exciton transfer. The effect of strong exciton-phonon coupling is described using an exciton-hopping superoperator calculated perturbatively in the off-diagonal exciton-phonon coupling. Since the diagonal exciton-phonon coupling is treated nonperturbatively, polaron formation and the nuclear reorganization energies are properly incorporated, in full analogy with Marcus electron transfer theory.[22] The signatures of exciton population dynamics in three-pulse echo and pump-probe measurements in light-harvesting antenna complexes are then explored using this theory.

The paper is organized as follows: In Section II we present the exciton Hamiltonian in the molecular (real space) basis and partition the third order response function into a coherent and a sequential component. Exact formal expressions for both components are derived in Appendix A using projection operator techniques. In Section III we transform the Hamiltonian into the delocalized exciton basis and calculate both contributions perturbatively in the off-diagonal exciton-phonon coupling. Details are given in Appendices B and C. Our final expressions, summarized in Appendix D, are applied in Section IV to the interpretation of photon echo and pump-probe signals in the B850 band of LH2. Our calculations include time-resolved and time-integrated echoes, echo peak-shift[14–16] (obtained from time-integrated detection), and spectrally-resolved pump-probe signals.[10–13] Finally our results are discussed in Section V.

II. THE DOORWAY/WINDOW REPRESENTATION OF THE THIRD-ORDER RESPONSE

We describe an aggregate made out of two-level molecules using the Frenkel-exciton Hamiltonian[17,18]

$$H = \sum_n \Omega_n \bar{B}_n^\dagger \bar{B}_n + \sum_{mn}^{m \neq n} J_{mn} \bar{B}_m^\dagger \bar{B}_n - \sum_{mn} q_{mn}^{(c)} \bar{B}_m^\dagger \bar{B}_n + H_{ph},$$

$$(1)$$

where $\bar{B}_n^\dagger$ ($\bar{B}_n$) are exciton creation (annihilation) operators for the n'th molecule, which satisfy the commutation relations

$$[\bar{B}_m, \bar{B}_n^\dagger] = \delta_{mn}(1 - 2\bar{B}_m^\dagger \bar{B}_m).$$

$$(2)$$

The polarization operator P representing coupling of the aggregate to the optical field $-E(t) \cdot P$ has a form

$$P = \sum_m d_m(\bar{B}_m + \bar{B}_m^\dagger).$$

$$(3)$$

The system is further coupled to a bath representing the molecular and the surrounding (solvent, protein, etc.) nuclear degrees of freedom. We shall represent them using a harmonic phonon Hamiltonian

$$H_{ph} = \sum_j \left(\frac{p_j^2}{2m_j} + \frac{m_j \omega_j^2 q_j^2}{2} \right).$$

$$(4)$$

$q_{mn}^{(c)}$ are collective bath coordinates, responsible for the exciton-phonon coupling

$$q_{mn}^{(c)} \equiv \sum_j m_j \omega_j^2 z_{j,mn} q_j,$$

$$(5)$$

where $z_{j,mn}$ is the coupling strength of j'th phonon to the exciton variable $\bar{B}_m^\dagger \bar{B}_n$.

All relevant information about the exciton-phonon interaction is contained in the following matrix of spectral densities

$$C_{mn,kl}(\omega) \equiv \frac{i}{2} \int_{-\infty}^{\infty} dt \exp(i\omega t) \langle [q_{mn}^{(c)}(t), q_{kl}^{(c)}(0)] \rangle, \quad (6)$$

where the expectation value and the time evolution in the r.h.s. of Eq. (6) are taken with respect to the free phonon Hamiltonian H_{ph}. As shown in the appendices, all effects induced by the exciton-phonon coupling on the general third-order response may be incorporated through the matrix of line broadening functions $g(t)$, which are related to the phonon spectral densities by[23]

$$g_{mn,kl}(t) \equiv \int_{-\infty}^{\infty} \frac{d\omega}{2\pi} \frac{1 - \cos(\omega t)}{\omega^2} \coth\left(\frac{\hbar\omega}{2kT}\right) C_{mn,kl}(\omega)$$

$$+ i \int_{-\infty}^{\infty} \frac{d\omega}{2\pi} \frac{\sin(\omega t) - \omega t}{\omega^2} C_{mn,kl}(\omega).$$

$$(7)$$

The time-domain optical response function $\hat{R}(t_3, t_2, t_1)$ which relates the third-order nonlinear polarization $P^{(3)}(t)$ to the driving field $E(t)$ is defined by (assuming that pulse 1 comes first, then pulse 2 and pulse 3 is the last)[23]

$$P^{(3)}(t) = \int_0^{\infty} dt_3 \int_0^{\infty} dt_2 \int_0^{\infty} dt_1 \hat{R}(t_3, t_2, t_1)$$

$$\times E_3(t - t_3) E_2(t - t_3 - t_2) E_1(t - t_3 - t_2 - t_1).$$
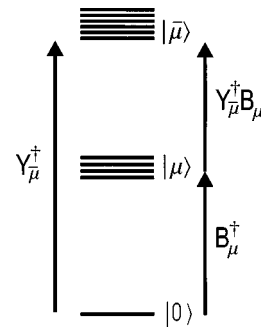
$$(8)$$

FIG. 1. Exciton level-structure and transition-dipoles of an aggregate made out of an N interacting two-level molecules. $|0\rangle$ is the ground state, $|\mu\rangle$ is the single exciton band which has N states and $|\bar{\mu}\rangle$ is the two-exciton band with $N(N-1)/2$ states. The operators inducing transitions between bands are displayed as well.

Since the Hamiltonian (Eq. (1)) conserves the number of excitons, the electronic states of the system which participate in the third order response are limited to the ground state 0, the single exciton $\{\mu\}$ and the two-exciton $\{\bar{\mu}\}$ manifolds (Fig. 1). During the t_1 period the system's density matrix is in an optical single-exciton coherence ($\rho_{0\mu}, \rho_{\mu0}$), whereas during t_3 it can be in $\rho_{\mu0}, \rho_{0\mu}, \rho_{\mu\bar{\mu}}$ and $\rho_{\bar{\mu}\mu}$. During the time interval t_2 the system is either in the one-exciton manifold $\rho_{\mu\nu}$, or in the ground state ρ_{00}, or in a two-exciton coherence $\rho_{0\bar{\mu}}, \rho_{\bar{\mu}0}$.

Formal expressions for the third-order optical response function can be obtained using projection operator techniques and following the procedure used in Ref. 19 to calculate the time- and frequency-resolved fluorescence. We then obtain (see Appendix A for derivation)

$$\hat{R}(t_3, t_2, t_1) = R^{(c)}(t_3, t_2, t_1)$$

$$+ \sum_{\mu\nu} \int_0^{t_2} dt'' \int_0^{t''} dt' \bar{W}_\mu(t_3, t_2 - t'')$$

$$\times G_{\mu\nu}(t'' - t') \bar{D}_\nu(t', t_1) + W_0(t_3) D_0(t_1).$$

$$(9)$$

The physical significance of these three terms is as follows: the first term represents a coherent contribution whereby the entire optical process is completed before a relaxed exciton population is created. The following two terms represent sequential (incoherent) contributions, expressed using the doorway-window representation.[19,23] The second term gives the contribution of thermally-relaxing excitons. The doorway function $\bar{D}_\nu$ represents the population of the νth exciton created after two interactions with the radiation field. $G_{\mu\nu}(t'' - t')$ is the conditional probability for the νth exciton to hop to the μth exciton state during $t'' - t'$. $\bar{W}_\mu$ is the window function representing the contribution of the μth exciton to the signal. The third term represents a Raman-type contribution whereby the system is back in the ground-state (ρ_{00}) during t_2. D_0 and W_0 are the corresponding ground state doorway and window functions. This term only gives the contribution for long t_2 (which is independent on t_2). The short time ground-state dynamics is contained in $R^{(c)}$. We shall refer to the three terms in Eq. (9) as the coherent,

the hopping and the bleaching terms respectively. Exact formal expressions for all quantities are given in Appendix A.

III. EXCITON VARIABLES FOR THE NONLINEAR RESPONSE

The eigenstates of the Hamiltonian (Eq. (1)) consist of well-separated manifolds of n exciton states $n = 0,1,2,\ldots$. As indicated earlier, the third-order response only depends on the ground state 0, the single exciton (μ) and the two-exciton ($\bar{\mu}$) states. To focus on these relevant states we shall recast the Hamiltonian using the exciton representation. To that end we introduce one-exciton $B_\mu^\dagger$ (B_μ) and two-exciton $Y_{\bar{\mu}}^\dagger$ ($Y_{\bar{\mu}}$) creation (annihilation) operators with $\mu = 1,\ldots,N$ and $\bar{\mu} = 1,\ldots,N(N-1)/2$, where N is the number of molecules in the aggregate. The one- and two-exciton operators are defined by[24]

$$B_\mu^\dagger |0\rangle \equiv \sum_n \varphi_\mu(n) \bar{B}_n^\dagger |0\rangle, \quad B_\mu^\dagger \bar{B}_m^\dagger |0\rangle = 0,$$

$$Y_{\bar{\mu}}^\dagger |0\rangle \equiv \sum_{mn} \Psi_{\bar{\mu}}(m,n) \bar{B}_m^\dagger \bar{B}_n^\dagger |0\rangle, \quad Y_{\bar{\mu}}^\dagger \bar{B}_m^\dagger |0\rangle = 0. \tag{10}$$

$|0\rangle$ is the electronic ground state. $\varphi_\mu(n)$ and $\Psi_{\bar{\mu}}(m,n)$ represent the one- and two-exciton eigenstates of the exciton Hamiltonian, with energies ϵ_μ and $\epsilon_{\bar{\mu}}$ respectively, and $\bar{B}_m^\dagger$ ($\bar{B}_m$) is the creation (annihilation) operator for an exciton at site m. It follows from Eq. (10) that $B_\mu^\dagger B_\nu^\dagger |0\rangle = 0$, which implies that two-exciton states are obtained from the ground-state by acting with two-exciton creation operators $Y_{\bar{\mu}}^\dagger$ rather than using bilinear combinations of one-exciton creation operators. The one- and two-exciton operators are defined such that B_μ and $B_\mu^\dagger$ have nonzero matrix elements between the ground and the one-exciton states whereas $Y_{\bar{\mu}}$ and $Y_{\bar{\mu}}^\dagger$ only couple the ground and two-exciton states. Operators which create two-exciton states by acting on one-exciton states are represented by $Y_{\bar{\mu}}^\dagger B_\mu$ (see Fig. 1).

Using these operators, the material Hamiltonian (Eq. (1)) assumes the form

$$H = H_0 + H_1, \tag{11}$$

with

$$H_0 \equiv \sum_\mu \epsilon_\mu B_\mu^\dagger B_\mu + \sum_{\bar{\mu}} \epsilon_{\bar{\mu}} Y_{\bar{\mu}}^\dagger Y_{\bar{\mu}} + \sum_\mu q_\mu^{(c)} B_\mu^\dagger B_\mu$$

$$+ \sum_{\bar{\mu}} q_{\bar{\mu}}^{(c)} Y_{\bar{\mu}}^\dagger Y_{\bar{\mu}} + H_{ph},$$

$$H_1 \equiv \sum_{\mu\nu}^{\mu \neq \nu} q_{\mu\nu}^{(c)} B_\mu^\dagger B_\nu + \sum_{\bar{\mu}\bar{\nu}}^{\bar{\mu} \neq \bar{\nu}} q_{\bar{\mu}\bar{\nu}}^{(c)} Y_{\bar{\mu}}^\dagger Y_{\bar{\nu}}. \tag{12}$$

The first two terms in H_0 represent one-exciton and two-exciton energies, the following two terms are related to diagonal coupling of the bath to one- and two-exciton states, whereas H_{ph} is the bath (phonon) Hamiltonian. H_1 denotes off-diagonal coupling of the bath to one- and two-exciton states.

Using these exciton variables, the polarization operator P (Eq. (3)) is given by

$$P = \sum_\mu d_\mu (B_\mu + B_\mu^\dagger) + \sum_{\mu\bar{\mu}} d_{\mu,\bar{\mu}} (Y_{\bar{\mu}}^\dagger B_\mu + B_\mu^\dagger Y_{\bar{\mu}}), \tag{13}$$

with the transition dipole matrix elements[21(a)]

$$d_\mu = \sum_m d_m \varphi_\mu(m),$$

$$d_{\mu,\bar{\mu}} = \sum_{mn} \Psi_{\bar{\mu}}(m,n)[\varphi_\mu(m) d_n + \varphi_\mu(n) d_m]. \tag{14}$$

The collective coordinates $q_{mn}^{(c)}$ have now been transformed into $q_\mu^{(c)}$, $q_{\bar{\mu}}^{(c)}$, $q_{\mu\nu}^{(c)}$, and $q_{\bar{\mu}\bar{\nu}}^{(c)}$. We shall denote these new collective variables as $q_{\bar{m}}^{(c)}$ where $\bar{m}$ assumes the values μ, $\bar{\mu}$, $\mu\nu$, and $\bar{\mu}\bar{\nu}$. Similarly the matrix of spectral densities Eq. (6) is now transformed into

$$C_{\bar{m}\bar{n}}(\omega) \equiv \frac{i}{2} \int_{-\infty}^{\infty} dt \exp(i\omega t) \langle [q_{\bar{m}}^{(c)}(t), q_{\bar{n}}^{(c)}(0)] \rangle, \tag{15}$$

where the expectation value and the time evolution in the r.h.s. of Eq. (15) are taken with respect to the phonon Hamiltonian H_{ph}. The transformation from $q_{mn}^{(c)}$ and $C_{mn,kl}(\omega)$ to $q_{\bar{m}}^{(c)}$ and $C_{\bar{m}\bar{n}}(\omega)$ is given by Eqs. (A1) and (A5) of Ref. 21(a).

Starting with Eq. (9), we have calculated all quantities to lowest order in H_1 and obtained

$$\hat{R}(t_3,t_2,t_1) = R^{(c)}(t_3,t_2,t_1) + \sum_{\mu\nu} W_\mu(t_3) G_{\mu\nu}(t_2) D_\nu(t_1)$$

$$+ W_0(t_3) D_0(t_1). \tag{16}$$

A closed expression for $R^{(c)}$ is derived in Appendix B by starting with its exact formal expression (Eq. (A13)) and expanding it to zeroth order in H_1.[21(a)] Turning now to the second term, exact formal definitions of $\bar{D}$ and $\bar{W}$ are given by Eqs. (A14) and (A17). To zeroth order in H_1, they can be expressed in terms of correlation functions (Eqs. (C3) and (C4)). These correlation functions are then evaluated using the second-order cumulant expansion and finally assume the forms of Eqs. (C2), (C12) and (C13). $G_{\mu\nu}(t_2)$ in the second term is the Green function of the generalized master equation for exciton-hopping (Eq. (A23)). Assuming short memory of the bath, $G_{\mu\nu}(t)$ satisfies the ordinary master equation (see Appendix A)

$$\frac{d}{dt} G_{\mu\nu}(t) = \sum_\alpha^{\alpha \neq \mu} [K_{\mu\alpha} G_{\alpha\nu}(t) - K_{\alpha\mu} G_{\mu\nu}(t)], \tag{17}$$

with the initial condition $G_{\mu\nu}(0) = \delta_{\mu\nu}$. The kernel $K_{\mu\nu}$ (Eq. (A24) together with Eq. (A22)) is evaluated to second order in H_1, resulting in Eqs. (C6) and (C7). These correlation functions can then be evaluated using the second-order cumulant expansion, resulting finally in Eqs. (C17)–(C19).

The last term in Eq. (9) may be calculated from Eq. (C5). Note that this term may be canceled by an identical term that appears in $R^{(c)}$ (Eq. (B9)). This could result in a more compact final expression. However, with the present
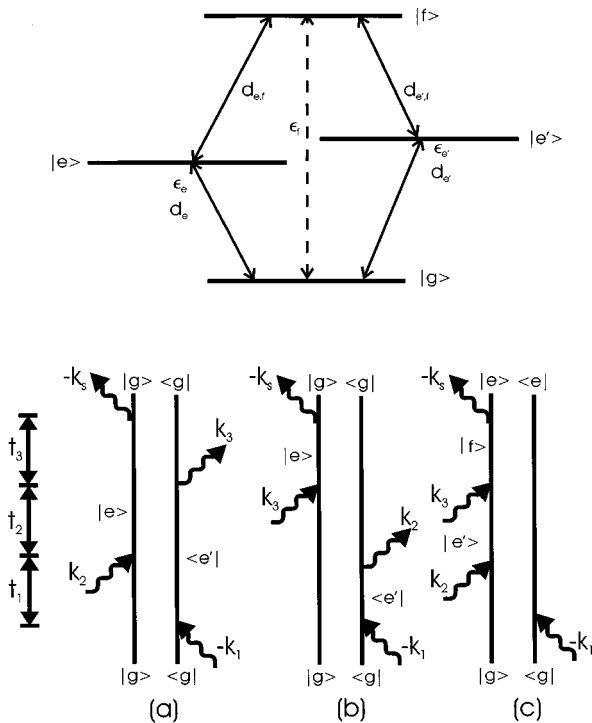
FIG. 2. Top: Excitonic four-level system consisting a ground (g), two one-exciton (e,e'), and one two-exciton states (f). The third-order response of an aggregate is a sum of contributions from various groups of four-level systems. Bottom: The three double-sided Feynman-diagrams representing the time domain four-wave mixing (three-pulse echo) within the rotating wave approximation. The bleaching term in Eq. (16) [Eq. (D6)] is represented by (b). The hopping term in Eq. (16) [Eq. (D7)] is represented by (a) and (c). The coherent term $R^{(c)}$ has five contributions [Eq. (B9) together with Eq. (D1)]. The first three R_I, R_{II} and R_{III} [Eqs. (D2)–(D4)] are represented by (a), (b), (c) respectively. The other two are the exciton hopping at $t_2 \to \infty$ and the bleaching term.

partitioning, $R^{(c)}$ vanishes for large t_2 and the second and the third term represent the long-time response.

IV. APPLICATION TO THE B850 SYSTEM OF LH2

Hereafter we consider a three-pulse experiment, where the incoming field is given by[25,26]

$$E(t) = E_1(t)(e^{i\mathbf{k}_1 \cdot \mathbf{r} - i\omega_1 t} + e^{-i\mathbf{k}_1 \cdot \mathbf{r} + i\omega_1 t}) + E_2(t)(e^{i\mathbf{k}_2 \cdot \mathbf{r} - i\omega_2 t}$$
$$+ e^{-i\mathbf{k}_2 \cdot \mathbf{r} + i\omega_2 t}) + E_3(t)(e^{i\mathbf{k}_3 \cdot \mathbf{r} - i\omega_3 t} + e^{-i\mathbf{k}_3 \cdot \mathbf{r} + i\omega_3 t})$$
$$\equiv E_1^+(t)e^{-i\omega_1 t} + E_1^-(t)e^{i\omega_1 t} + E_2^+(t)e^{-i\omega_2 t} + E_2^-(t)e^{i\omega_2 t}$$
$$+ E_3^+(t)e^{-i\omega_3 t} + E_3^-(t)e^{i\omega_3 t}, \tag{18}$$

where $E_i(t)$ are the real pulse envelopes. E_i^+ (E_i^-) refer to the components of E with directions $+\mathbf{k}_i$ ($-\mathbf{k}_i$). In the following we focus on impulsive three-pulse four-wave mixing (FWM) experiments where pulse 1 comes at time $-t_1 - t_2$, pulse 2 comes at time $-t_2$, and pulse 3 at time 0. The signal is observed in the direction $\mathbf{k}_s = \mathbf{k}_3 + \mathbf{k}_2 - \mathbf{k}_1$. For pulses short compared with all molecular time scales (except for the optical frequencies), we can replace the pulse envelopes in Eq. (8) by δ functions and eliminate the time integrations, provided we invoke the rotating-wave-approximation (RWA), i.e. neglect highly oscillating terms in $\hat{R}$.[23] We finally obtain

$$P^{(3)}(t_3) = E_1^- E_2^+ E_3^+ \theta(t_3) \theta(t_2) \theta(t_1) \hat{R}(t_3, t_2, t_1), \tag{19}$$

where $\hat{R}(t_3, t_2, t_1)$ within the RWA is given in Appendix D. The polarization now depends on three positive time variables: the time delay t_1 between pulses 1 and 2, the time delay t_2 between pulses 2 and 3, and the time of observation t_3.

All numerical calculations were performed using Eq. (19), where $\hat{R}(t_3, t_2, t_1)$ is given by Eq. (16) with all necessary quantities collected in Appendix D. $R^{(c)}$ is calculated using Eqs. (D1)–(D6). The exciton-hopping term (the second term of Eq. (16)) was evaluated using Eq. (D7). The bleaching contribution (the last term of Eq. (16)) was calculated using Eq. (D6).

We consider a cyclic aggregate made out of N molecules with nearest-neighbor intermolecular interactions. This model describes light-harvesting LH1 antenna complexes, as well as the B850 and B800 bands of LH2, which are highly symmetric circular one-dimensional aggregates with $N = 32$, 18, and 9, respectively. It further represents J-aggregates which have a linear geometry and large N. We have used the coupling J between adjacent chlorophyll molecules as determined in Ref. 27 -273 cm^{-1} and -291 cm^{-1} for the B850 system of LH2, which is a ring consisting of 18 Bchl-a monomers.[28] For nearest-neighbor intermolecular coupling, the many-exciton states are represented by the Bethe Ansatz[21(a),29] and can be expressed in terms of two sets of one-exciton states: ordinary one-exciton states $\varphi_\mu(n)$ satisfying periodic boundary conditions $\varphi_\mu(n+N) = \varphi_\mu(n)$, and auxiliary one-exciton states $\bar{\varphi}_\mu(n)$ with antiperiodic boundary conditions $\bar{\varphi}_\mu(n+N) = -\bar{\varphi}_\mu(n)$, both are eigenstates of the one-exciton Hamiltonian with energies ϵ_μ and $\bar{\epsilon}_\mu$, respectively.[21(a)] We assume that all the collective phonon variables acting on different molecules are uncorrelated and have the same spectral density. This gives

$$C_{mn,kl}(\omega) = \delta_{mk} \delta_{nl} \delta_{mn} C(\omega). \tag{20}$$

The combined effects of disorder and exciton-phonon coupling characterized by the nuclear spectral densities on two-pulse echoes were analyzed in Ref. 21(a) using five models involving different spectral densities and different models of disorder. Hereafter we use the spectral density of model I in Ref. 21(a), corresponding to an overdamped Brownian oscillator.

$$C(\omega) = 2\lambda \frac{\omega \tau_1}{\omega^2 \tau_1^2 + 1}, \tag{21}$$

with $\tau_1 = 130$ fs. We further include disorder by assuming a Gaussian distribution of molecular frequencies Ω_n with a FWHM of σ. The linear absorption linewidth is determined by homogeneous and inhomogeneous contributions, represented by λ and σ, respectively. This linewidth as well as the long-time pump-probe signal do not carry enough information to determine these parameters uniquely, and may be
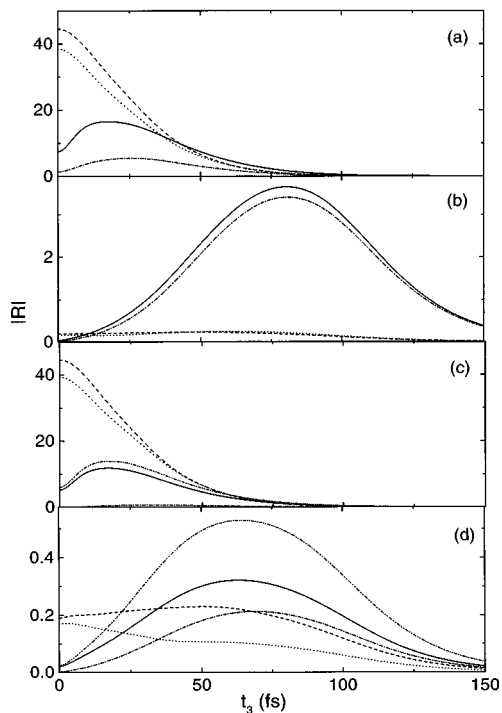
FIG. 3. Square root of time-resolved echo signals $|R(t_3,t_2,t_1)|$ (Eq. (22)) versus the observation time t_3, (a) $t_2=t_1=0$, (b) $t_2=0$, $t_1=100$ fs, (c) $t_2=200$ fs, $t_1=0$, and (d) $t_2=200$ fs, $t_1=100$ fs. Total signal (solid), bleaching (dashed), exciton-hopping term (dotted), coherent component (dashed-dotted). In (c) and (d) we also show the sum of the coherent and bleaching term (dash-dot-dot).

reproduced with different choices.[20(b)] The parameters used $\lambda=240$ cm^{-1} and $\sigma=600$ cm^{-1}, reproduce the experimental $\Gamma\approx470$ cm^{-1} (FWHM) linear absorption linewidth, and the three-pulse echo peak-shift,[15] as will be shown below. All calculations were performed for $T=300$ K. The calculated signals have been averaged over 1000 realizations of static disorder, which is sufficient for the short-times and time-delays considered here. Considerably more extensive sampling is required for longer times or time-delays.

A. Time-resolved three pulse echoes

The time-resolved four-wave-mixing signal is given by

$$S_{3PE}(t_3,t_2,t_1)\propto|\hat{R}(t_3,t_2,t_1)|^2. \tag{22}$$

The absolute value of $\hat{R}(t_3,t_2,t_1)$ for different t_2 and t_1 is displayed in Fig. 3. For $t_1=t_2=0$ (Fig. 3(a)) there are large, initially almost canceling, contributions from the bleaching and the term involving exciton hopping. This cancellation comes from the fact that the two-exciton contributions dominate the latter term whereas the bleaching involves only single-exciton states, which have a different sign[21(a)] (see also the pump probe signal displayed in Fig. 6(a)). With increasing t_3 this strong cancellation is partially eroded, due to the different frequencies of the ground state to one-exciton compared to the single-exciton to two-exciton transitions. The total signal therefore reaches its maximum around $t_3\approx17$ fs and subsequently decays due to homogeneous and inhomogeneous dephasing. The coherent component is rather weak in Fig. 3(a). With increasing t_1, (see Fig. 3(b) for $t_2=0$

and $t_1=100$ fs), both the bleaching and the exciton hopping term vanish rapidly. Also the coherent component decays as with t_1, but not as rapidly as the other terms, since it evolves into a photon echo. The total signal which is much weaker than for $t_1=0$ closely resembles to the coherent component.

The echo signal reaches a maximum at about 80 fs, which is shorter than the ideal value of $t_1=100$ fs expected for a two-level model. This difference is due to the fact that in addition to the disorder-induced inhomogeneous broadening which results in the echo, phonon-induced homogeneous dephasing is present as well. Homogeneous dephasing leads to a decay of the signal which pushes the echo towards earlier times.[21(a)] With increasing t_2, (see Fig. 3(c) for $t_2=200$ fs and $t_1=0$ fs) the bleaching does not change at all, and the term involving exciton-hopping changes only slightly. However the coherent component decays rapidly with t_2, which is to be expected since it vanishes for long t_2. In Fig. 3(c) the total signal and, the signal calculated by neglecting exciton hopping are quite close, and both are smaller than the total signal calculated for $t_2=0$ fs (see Fig. 3(a)).

Figure 3(d) displays the signals for $t_2=200$ fs and $t_1=100$ fs. For these time delays the two contributions are comparable, but due to cancellations between the bleaching and the exciton hopping term, the shape of the total signal is similar to the coherent component. Both total signals calculated with and without exciton hopping show a photon echo with a maximum at about 63 fs and 65 fs, respectively. This is earlier than the 80 fs maximum shown in Fig. 3(b). Therefore during the time period t_2 the relative magnitude of the inhomogeneous broadening compared with the homogeneous dephasing decreases; this effect is stronger if exciton hopping is included. Due to the strong overall decay of the coherent component during t_2, the total signal shown in Fig. 3(d) is also weaker than that shown in Fig. 3(b).

B. Time-integrated echoes and peak-shift signals

The photon echo technique does not always produce an echo signal: this depends on the nature of the system and the line broadening mechanism.[23] The echo can be observed by time-resolved detection as shown in the previous subsection. However, characteristic signatures of the echo are contained in the simpler (and more common) time-integrated detection. The time-integrated signal is given by

$$S_{INT}(t_1,t_2)=\int_{-\infty}^{\infty}|\hat{R}(t_3,t_2,t_1)|^2 dt_3. \tag{23}$$

In Fig. 4 we display this signal as a function of t_1 for different values of t_2. For a homogeneously-broadened two-level system, whose real-time signal is characterized by an exponential decay, this signal reaches its maximum at $t_1=0$ irrespective of the value of t_2 and then decays exponentially. For an ensemble of inhomogeneously broadened two-level systems, the real-time signal appears as a photon echo, i.e. has its maximum at $t_3=t_1$.[23,30] In the absence of homogeneous dephasing, the time-integrated signal will start with some value at $t_1=0$ and then as function of t_1 will rise to a constant value, which is reached when t_1 becomes larger
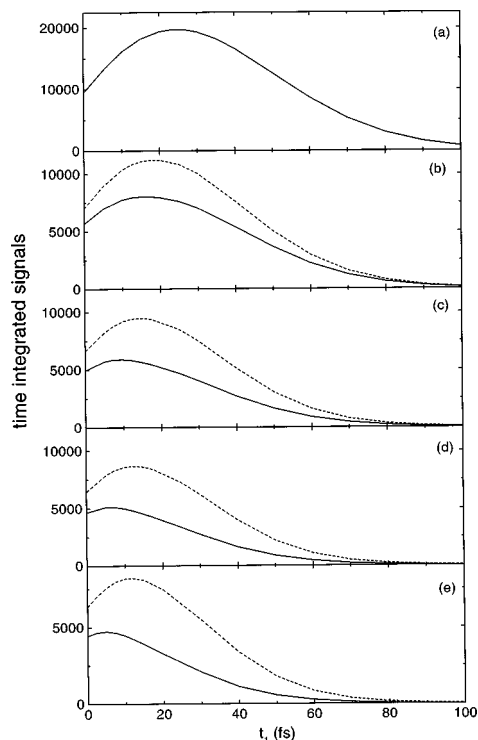
FIG. 4. Time-integrated echo signals S_{INT} (Eq. (23)) versus t_1 for (a) $t_2=0$, (b) $t_2=50$ fs, (c) $t_2=100$ fs, (d) $t_2=150$ fs, and (e) $t_2=200$ fs. Shown are the total signals (solid line) and the sum of the coherent and bleaching term (dashed line).

FIG. 5. Echo peak shift t_1^* as function of the delay t_2. Circles—calculated peak shifts; uptriangles—calculated peak shifts if the exciton-hopping term is neglected (keeping only the coherent and bleaching components in Eq. (16)); squares—experiment (Ref. 15(b)).

than the temporal width of the time-resolved echo signal. This behavior comes from the fact that for an inhomogeneously broadened system, for time-delays t_1 which are shorter than the temporal width of the echo signal, part of the photon echo is cut off and does not contribute to the signal, which only starts after the last pulse. With increasing t_1, a larger portion of the echo signal contributes, and the time-integrated signal rises. Including homogeneous dephasing, the time-integrated signal will eventually decay to zero. The signal will therefore show a maximum at some t_1^* (denoted the peak-shift) equal to or smaller than the temporal width of the echo. The precise value of t_1^* is determined by the ratio of the width of the echo (inhomogeneous broadening) and the homogeneous dephasing time, as well as the delay period t_2. Peak-shift measurements provide some valuable information about the temporal behavior of the time-resolved signal, even though a time-integrated detection is used.[14–16]

Peak-shift signals have been reported for LH1, for the B850 band of LH2, and for the B800 band of LH2 as function of the time-delay t_2. In Ref. 15 it was found that for both LH1 and LH2 it decays as function of t_2, and experiments could be fitted by using a simple model where the entire aggregate is represented by a two electronic level system coupled to a complex spectral density representing seven nuclear modes. Peak-shift measurements for the B820 dimer subunit of LH1[15(c)] could then be fitted with the same coupling to nuclear modes, neglecting one term associated with energy-transfer. The larger values of the peak-shift of the dimer compared to LH1 were explained by assuming that in LH1 the peak-shift is destroyed by energy transfer processes,
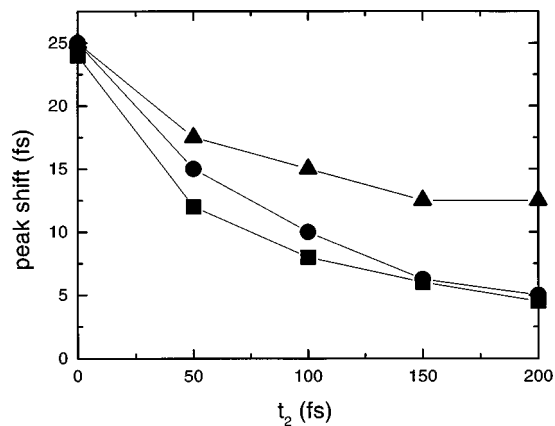
which are negligible in the dimer. This simple model completely neglects the detailed structure of the excitonic manifold and the influence of two-exciton states. It further includes relaxation as well as disorder effects only through a line shape function introduced phenomenologically.

In Fig. 4 we display the calculated time-integrated signal as a function of t_1 for different t_2. For $t_2=0$ we find the maximum of the time-integrated signal at $t_1=25(\pm 2.5)$ fs (the uncertainty represents the finite grid of t_1 values used in the calculation). With increasing t_2 the maximum shifts towards shorter t_1. We further display the signals obtained by neglecting exciton hopping altogether (note that for impulsive excitation, no exciton hopping takes place for $t_2=0$), i.e. by setting $G_{\mu\nu}(t)=\delta_{\mu\nu}$ in Eq. (16). Without exciton-hopping we notice somewhat stronger signals, and the maximum shifts towards larger values of t_1.

The calculated peak-shifts for $t_2=0$, 50, 100, 150, 200 fs are displayed in Fig. 5. These values are very close to experiment.[15(b)] This agreement is encouraging, despite several approximations made: We have used a very simple spectral density of a single overdamped Brownian oscillator and neglected the effects of the finite pulse durations. In addition, a more realistic model should consider an aggregate made out of three level (rather than two level) chromophores. The doubly-excited (third) molecular state may couple strongly to the two-exciton manifold and influence the third-order response.[10] A unified description of all spectroscopic measurements (including pump-probe, hole-burning, etc.) may require relaxing some of these approximations. Figure 5 also shows that exciton-hopping reduces the magnitude of the peak-shift, especially for long t_2. We therefore conclude that the general idea that exciton-hopping is responsible for reducing the peak-shift to small values at long times as outlined in Ref. 16 is qualitatively correct. As shown in the previous section, even for a large t_2, and t_1 larger than t_1^* (see Fig. 3(d)) the time-resolved signals are still emitted as echoes with a width much larger than t_1^*. Therefore the decay of t_1^* between $t_2=0$ to 200 fs is rather related to an increase of the overall dephasing and not so much to a loss of rephasing capability (effective inhomogeneous broaden-
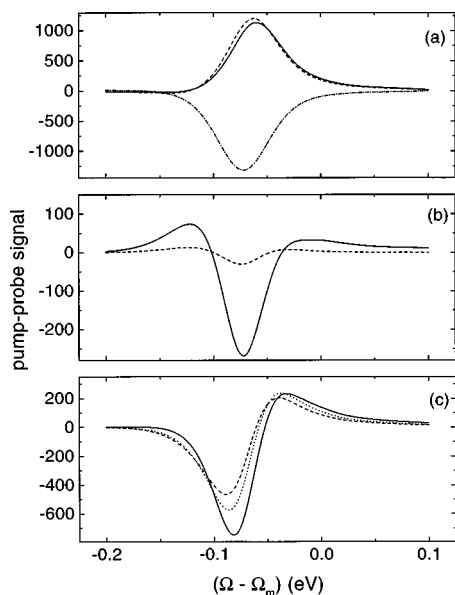
FIG. 6. Impulsive pump-probe signals S_{pp} (Eq. (24)). Panel (a): dotted-dashed line—bleaching term; solid line—exciton-hopping term when $t_2 = 0$; dashed line—exciton-hopping term when $t_2 = 200$ fs. Panel (b): solid line—coherent term, $t_2 = 0$; dashed line—coherent term, $t_2 = 200$ fs. Panel (c): solid line—total signal, $t_2 = 0$; dashed line—total signal, $t_2 = 200$ fs; dotted line—sum of the coherent and bleaching term, $t_2 = 200$ fs.

ing). This is illustrated by the decay of the time-integrated signal (see Fig. 4) and the similar echo structure of the time-resolved signals shown in Figs. 3(b) and (d), as discussed above.

C. Pump-probe spectroscopy

Pump-probe measurements can be viewed as a specific four-wave-mixing process whereby pulses 1 and 2 coincide and the frequency-dispersed signal is measured. Assuming that both the pump and the probe are impulsive (very short), the signal is obtained by setting $t_1 = 0$ in Eq. (19) and performing a Fourier transform with respect to t_3:

$$S_{pp}(\omega, t_2) = \text{Im} \int_0^\infty dt_3 \exp(i\omega t_3) \hat{R}(t_3, t_2, 0). \quad (24)$$

Figure 6 displays the various contributions to the pump-probe signals for $t_2 = 0$ (solid line) and $t_2 = 200$ fs (dashed line). In panel (a) we plot the exciton-hopping and bleaching term [Eq. (16)], and panel (b) shows the coherent contribution. The total signal is displayed in panel (c). We find a strong negative bleaching contribution, which is independent of t_2 (dashed-dotted line in Fig. 6(a)). The hopping component is strong and positive, which shows that excited-state absorption representing transitions from one-exciton to two-exciton states dominates this component. The red-shift of the peak reflects the exciton-hopping during the t_2 period. The coherent component strongly depends on t_2 (see Fig. 6(b)), which reflects polaron formation, and almost vanishes after 200 fs. This component includes contributions from both bleaching and excited-state absorption. Their interference results in a strong negative signal with positive wings in the

blue and in the red, indicating the broader spectral width of the one- to two-exciton transition compared to the ground state to single-exciton transition.

The total signal displayed in Fig. 6(c) is weak compared to the individual contributions because of the strong cancellation between the negative bleaching term and the positive excited-state absorption. Since the positive (excited-state absorption) peak is shifted toward the blue compared to the minimum of the bleaching, the total signal shows a negative component at lower energies and a positive feature at higher energies (see Fig. 6(c)). Upon increasing t_2 the positive and negative peaks of the total signal slightly decrease (due to the coherent component) and shift toward the red (due to exciton-hopping). The dotted line in Fig. 6(c) is the total signal calculated by neglecting exciton-hopping. The difference from the actual signal (dashed-line) illustrates the importance of incorporating the hopping term, as shown in Fig. 4, Fig. 5, and Fig. 6(a).

V. DISCUSSION

The theory presented in this paper incorporates exciton relaxation processes in nonlinear spectroscopies of molecular aggregates. The theory accounts for strong energetic disorder and exciton-phonon coupling and applies when the disorder-induced exciton localization length is shorter than the phonon-induced exciton self-trapping length (polaron size) in the absence of disorder. Exciton transport is described by a master equation. The present theory generalizes our earlier calculations: the two-pulse echo is related to $\hat{R}(t_3, 0, t_1)$, which has been calculated previously in Ref. 21(a) by neglecting H_1 and including effects of polaron formation. However, since H_0 conserves exciton populations, it completely neglects exciton-hopping, which takes place during the t_2 period and may not be neglected for long t_2, even when H_1 is weak. In this article we have extended these results to three-pulse measurements with finite t_2, by treating H_1 perturbatively.

We have applied this theory to calculate the four wave mixing signal in LH2. The total signal consists of three terms denoted the coherent, exciton-hopping and bleaching contributions. Our calculations show that polaron formation and hopping occur during the time delay period t_2, which can be controlled in three-pulse-echo and pump-probe measurements. The results for the peak-shift measurements are in good agreement with recent experiments.[15] In addition this approach can be extended for calculating the time- and frequency-resolved spontaneous emission using the formalism of Ref. 19.

All calculations were performed for LH2 in one particular species of bacterium *Rhodopseudomonas (Rps.) acidophila* where B850 system has $N = 18$ chlorophylls. This number varies for different species (e.g. for *Rhodospirillum (Rs.) molischianum* it is 16). The precise shape of the time-resolved signals will depend on N, since it affects the nature of the exciton states, as well as the influence of the disorder and effective exciton phonon coupling. However the general expressions and the existence of almost canceling terms (see also Ref. 21(a)) apply for any N. Since for the parameters

used in the present paper, the exciton states are localized due to static disorder on a small number of sites (compared to N), we do not expect strong changes by varying N, as long as it is larger than the exciton localization length of approximately 4 chlorophylls.

The calculations presented here and in Ref. 21(a) demonstrate that time-resolved FWM signals from light-harvesting aggregates should be most valuable and provide direct information about the relative roles of homogeneous and inhomogeneous dephasing. This information is not available from time-integrated measurements.

In the present calculations we used a three band model (Fig. 1) to represent the system, and included exciton-phonon coupling as well as static-disorder. This model should apply to a broad class of organic and semiconductor excitonic materials; these include molecular aggregates, crystals and superlattice,[23] as well as semiconductors and semiconductor nanostructure.[31]

ACKNOWLEDGMENTS

APPENDIX A: COHERENT AND SEQUENTIAL COMPONENTS OF THE THIRD ORDER RESPONSE

In this Appendix we derive the doorway-window representation for the optical response function (Eq. (9)), using projection operator techniques.[32]

We start with the formal expression for the nonlinear response function[23]

$$\hat{R}(t_3, t_2, t_1) = i^3 \text{Tr}[P_+ \mathscr{G}(t_3) P_- \mathscr{G}(t_2) P_- \mathscr{G}(t_1) P_- \bar{\rho}_0],$$
(A1)

where $\bar{p}_0$ is the equilibrium density matrix and

$$\mathscr{G}(t) \equiv \exp(-iLt),$$
(A2)

with the Liouville operator L defined as $LA = [H, A]$, A being an arbitrary operator. $P_\pm$ are Liouville space dipole operators (superoperators). They are defined by their actions on an arbitrary operator A

$$P_- A \equiv PA - AP$$

$$P_+ A \equiv \frac{1}{2}[PA + AP].$$
(A3)

For calculating the third-order response we need to follow the evolution of the wave packets $\rho_{0\mu}(\mathbf{q})$, $\rho_{0\bar{\mu}}(\mathbf{q})$, $\rho_{\mu\bar{\nu}}(\mathbf{q})$, $\rho_{00}(\mathbf{q})$, and $\rho_{\mu\nu}(\mathbf{q})$, where $\mathbf{q}$ represents all the nuclear degrees of freedom. We shall introduce the following projection operator: $\mathscr{P}_\mu$ projects the density matrix onto the manifold of single-exciton populations

$$\mathscr{P}_\mu \rho \equiv \bar{\rho}_\mu(\mathbf{q}) \text{Tr}_\mathbf{q}(\rho_{\mu\mu}),$$
(A4)

where $\bar{\rho}_\mu(\mathbf{q})$ is the equilibrium density matrix for the Hamiltonian H_0 when the μth exciton is excited. We further introduce the operator $\mathscr{P}_0$ which projects the density matrix onto the ground state

$$\mathscr{P}_0 \rho \equiv \bar{\rho}_0(\mathbf{q}) \text{Tr}_\mathbf{q}(\rho_{00}),$$
(A5)

and $\rho_{00}(\mathbf{q})$ is the equilibrium density matrix in the ground state. The μ-dependence of $\bar{\rho}_\mu(\mathbf{q})$ reflects the different nuclear equilibrium for each electronic state and retains polaron effects.[33] (These are neglected in the standard derivation of master equations where weak exciton-phonon coupling is assumed and $\bar{\rho}_\mu(\mathbf{q})$ is replaced by a μ-independent nuclear density matrix).

Our total projection operator is defined by

$$\mathscr{P} = \sum_\mu \mathscr{P}_\mu + \mathscr{P}_0.$$
(A6)

$\mathscr{P}$ projects the density matrix onto the manifold of single-exciton populations as well as the ground state. $\mathscr{P}\rho = 0$ for all components except $\rho_{\mu\mu}(\mathbf{q})$ and $\rho_{00}(\mathbf{q})$. Using this projection, we can partition the density matrix ρ as $\rho = \mathscr{P}\rho + \mathscr{Q}\rho$, where $\mathscr{Q} \equiv (\text{I} - \mathscr{P})$ is the complementary projection to $\mathscr{P}$.

$\mathscr{P}$ represents our slow dynamical variables which we wish to follow explicitly. Acting with the unit operator $\mathscr{P} + \mathscr{Q}$ on $\mathscr{G}(t_2)$ in Eq. (A1), we obtain

$$\mathscr{G}(t_2) = (\mathscr{P} + \mathscr{Q})\mathscr{G}(t_2)(\mathscr{P} + \mathscr{Q})$$
$$\equiv \mathscr{G}_{\mathscr{P}\mathscr{P}}(t_2) + \mathscr{G}_{\mathscr{Q}\mathscr{Q}}(t_2) + \mathscr{G}_{\mathscr{P}\mathscr{Q}}(t_2) + \mathscr{G}_{\mathscr{Q}\mathscr{P}}(t_2),$$
(A7)

where we have introduced the abbreviated notation

$$\mathscr{G}_{\mathscr{A}\mathscr{B}}(t) \equiv \mathscr{A} \exp(-iLt)\mathscr{B},$$
(A8)

and $\mathscr{A}, \mathscr{B} = \mathscr{P}, \mathscr{Q}$.

We shall partition the Liouville operator as $L = L_0 + L_1$, where $L_0 \mathscr{P} = \mathscr{P} L_0 = 0$, $[\mathscr{P}, L] = 0$ and $\mathscr{P} L_1 \mathscr{P} = 0$. We can then use standard projection operator identities:

$$\mathscr{G}_{\mathscr{P}\mathscr{Q}}(t_2) = -i \int_0^{t_2} dt \, \mathscr{G}_{\mathscr{P}\mathscr{P}}(t_2 - t) L_1 \mathscr{Q} \tilde{\mathscr{G}}(t),$$
(A9)

$$\mathscr{G}_{\mathscr{Q}\mathscr{P}}(t_2) = -i \int_0^{t_2} dt \, \tilde{\mathscr{G}}(t_2 - t) \mathscr{Q} L_1 \mathscr{G}_{\mathscr{P}\mathscr{P}}(t),$$
(A10)

$$\mathscr{G}_{\mathscr{Q}\mathscr{Q}}(t_2) = \mathscr{Q} \tilde{\mathscr{G}}(t_2) \mathscr{Q} + (-i)^2 \int_0^{t_2} dt'' \int_0^{t''} dt' \, \tilde{\mathscr{G}}(t_2 - t'')$$
$$\times \mathscr{Q} L_1 \mathscr{G}_{\mathscr{P}\mathscr{P}}(t'' - t') L_1 \mathscr{Q} \tilde{\mathscr{G}}(t'),$$
(A11)

where $\tilde{\mathscr{G}}(t)$ is defined as

$$\tilde{\mathscr{G}}(t) \equiv \exp(-i\mathscr{Q}L\mathscr{Q}t).$$
(A12)

Equations (A9)–(A11) are the Fourier transforms of Eqs. (2.89b)–(2.89d) of Ref. 23. Substituting Eqs. (A7), and (A9)–(A11) into Eq. (A1) and representing $\mathscr{P}$ in the form of Eqs. (A4) and (A5) we obtain the DW representation for the nonlinear response function $\hat{R}$. It has the form of Eq. (9), where the coherent component is given by

J. Chem. Phys., Vol. 108, No. 18, 8 May 1998

Zhang *et al.* 7771

$$R^{(c)}(t_3,t_2,t_1)=i^3 \, \text{Tr}[P_+\bar{\mathscr{G}}(t_3)P_-\mathscr{G}(t_2)\mathcal{Q}P_-\mathscr{G}(t_1)P_-\bar{\rho}_0]. \tag{A13}$$

Given the dipole operators (Eq. (A3), it is clear that during the period of t_1 and t_3 the density matrix is in an optical coherence (i.e., $\rho_{0\mu}$). These states belong to the $\mathcal{Q}$ space since the projection operator $\mathscr{P}$ only includes populations. We can thus replace $\mathscr{G}(t_3)$ by $\bar{\mathscr{G}}(t_3)$ and $\mathscr{G}(t_1)$ by $\bar{\mathscr{G}}(t_1)$.

The doorway function can be represented formally as follows

$$\bar{D}_\nu(\tau,t)=D_\nu(t)\delta(\tau)+D_\nu^{(1)}(\tau,t), \tag{A14}$$

with

$$D_\nu(t)\equiv\text{Tr}[\mathscr{P}_\nu P_-\bar{\mathscr{G}}(t)P_-\bar{\rho}_0], \tag{A15}$$

$$D_\nu^{(1)}(\tau,t)\equiv-i\,\text{Tr}[\mathscr{P}_\nu L_1\bar{\mathscr{G}}(\tau)P_-\bar{\mathscr{G}}(t)P_-\bar{\rho}_0]. \tag{A16}$$

Similarly, the window function is given by

$$\bar{W}_\mu(t,\tau)=W_\mu(t)\delta(\tau)+W_\mu^{(1)}(t,\tau), \tag{A17}$$

with

$$W_\mu(t)\equiv-i\,\text{Tr}[P_+\bar{\mathscr{G}}(t)P_-\bar{\rho}_\mu], \tag{A18}$$

$$W_\mu^{(1)}(t,\tau)\equiv-\text{Tr}[P_+\bar{\mathscr{G}}(t)P_-\bar{\mathscr{G}}(\tau)L_1\bar{\rho}_\mu]. \tag{A19}$$

The Green function G represents the matrix elements of $\mathscr{G}_{\mathscr{P}\mathscr{P}}$,

$$G_{\mu\nu}(t)\equiv\mathscr{P}_\mu\exp(-iLt)\mathscr{P}_\nu, \tag{A20}$$

$G_{\mu\nu}(t)$ is the conditional probability for the population to be in the state μ at time t given that it started at state ν at $t=0$. It satisfies the generalized master equation.

$$\frac{d}{dt}G_{\mu\nu}(t)=\sum_\alpha\int_0^t dt'\,\bar{K}_{\mu\alpha}(t-t')G_{\alpha\nu}(t'), \tag{A21}$$

with initial condition $G_{\alpha\nu}(0)=\delta_{\alpha\nu}$. The kernel of this equation is given by:

$$\bar{K}_{\mu\nu}(t)\equiv-\text{Tr}[\mathscr{P}_\mu L_1\bar{\mathscr{G}}(t)L_1\bar{\rho}_\nu]. \tag{A22}$$

Conservation of the total polaron population allows to recast Eq. (A21) in a form

$$\frac{d}{dt}G_{\mu\nu}(t)=\sum_\alpha^{\alpha\neq\mu}\int_0^t dt'[\bar{K}_{\mu\alpha}(t-t')G_{\alpha\nu}(t') \\ -\bar{K}_{\alpha\nu}(t-t')G_{\mu\nu}(t')]. \tag{A23}$$

Invoking the Markovian approximation we obtain Eq. (17) with

$$K_{\mu\nu}\equiv\int_0^\infty dt\,\bar{K}_{\mu\nu}(t). \tag{A24}$$

D_0 and W_0 in Eq. (9) are given by

$$D_0(t)=\text{Tr}[\mathscr{P}_0 P_-\bar{\mathscr{G}}(\tau)P_-\bar{\rho}_0], \tag{A25}$$

$$W_0(t)=-i\,\text{Tr}[P_+\bar{\mathscr{G}}(\tau)P_-\bar{\rho}_0]. \tag{A26}$$

Equation (9) together with Eqs. (A13)–(A26) constitute an exact closed formal expression for the third-order response function.

APPENDIX B: THE COHERENT COMPONENT OF THE THIRD-ORDER RESPONSE

In this and in the following Appendices we derive perturbative expressions for all quantities which appear in Eq. (9). To that end, we set $\bar{\mathscr{G}}(t)\cong\bar{\mathscr{G}}_0(t)$ in the formal expressions given by Eqs. (A13)–(A19) and (A22), where

$$\bar{\mathscr{G}}_0(t)\equiv\exp(-i\mathcal{Q}L_0\mathcal{Q}t). \tag{B1}$$

Exact calculations can be performed since $\bar{\mathscr{G}}_0(t)$ is defined in the system with $H_1=0$. Representing $\mathcal{Q}$ in Eq. (A13) in a form $\mathcal{Q}=I-\mathscr{P}$ we obtain

$$R^{(c)}(t_3,t_2,t_1)=R(t_3,t_2,t_1)-R(t_3,\infty,t_1), \tag{B2}$$

where $R(t_3,t_2,t_1)$ is the response function for $H_1=0$. Formal expressions for R derived in Ref. 21(a) have the form

$$R(t_3,t_2,t_1)=\sum_{\alpha=1}^{4}\sum_{j=1}^{2}[R_{\alpha j}(t_3,t_2,t_1)-R_{\alpha j}^*(t_3,t_2,t_1)], \tag{B3}$$

with

$$R_{1j}(t_3,t_2,t_1)=F_j(t_1,t_1+t_2,t_1+t_2+t_3,0),$$

$$R_{2j}(t_3,t_2,t_1)=F_j(0,t_1+t_2,t_1+t_2+t_3,t_1),$$

$$R_{3j}(t_3,t_2,t_1)=F_j(0,t_1,t_1+t_2+t_3,t_1+t_2),$$

$$R_{4j}(t_3,t_2,t_1)=F_j(t_1+t_2+t_3,t_1+t_2,t_1,0). \tag{B4}$$

The correlation functions F_j can be evaluated exactly, using the matrix of line broadening functions and have the form[21(a),34]

$$F_1(\tau_4,\tau_3,\tau_2,\tau_1)=\sum_{\mu\nu}d_\mu^2 d_\nu^2\exp[-f_{\mu\nu}^{(1)}(\tau_4,\tau_3,\tau_2,\tau_1) \\ -i\epsilon_\mu(\tau_2-\tau_1)-i\epsilon_\nu(\tau_4-\tau_3)],$$

$$F_2(\tau_4,\tau_3,\tau_2,\tau_1)=\sum_{\mu\nu\bar{\alpha}}d_\mu d_\nu d_{\mu,\bar{\alpha}}d_{\nu,\bar{\alpha}} \\ \times\exp[-f_{\mu\nu,\bar{\alpha}}^{(2)}(\tau_4,\tau_3,\tau_2,\tau_1) \\ -i\epsilon_\mu(\tau_2-\tau_1)-i\epsilon_{\bar{\alpha}}(\tau_3-\tau_2) \\ -i\epsilon_\nu(\tau_4-\tau_3)], \tag{B5}$$

where $f^{(1)}$ and $f^{(2)}$ are given by

$$f_{\mu\nu}^{(1)}(\tau_4,\tau_3,\tau_2,\tau_1)\equiv g_{\mu\mu}(\tau_2-\tau_1)-g_{\mu\nu}(\tau_3-\tau_1) \\ +g_{\mu\nu}(\tau_4-\tau_1)+g_{\mu\nu}(\tau_3-\tau_2) \\ -g_{\mu\nu}(\tau_4-\tau_2)+g_{\nu\nu}(\tau_4-\tau_3), \tag{B6}$$

7772   J. Chem. Phys., Vol. 108, No. 18, 8 May 1998

Zhang *et al.*

$$f^{(2)}_{\mu\nu,\bar{\alpha}}(\tau_4,\tau_3,\tau_2,\tau_1)$$

$$\equiv g_{\mu\mu}(\tau_2-\tau_1)-g_{\mu\bar{\alpha}}(\tau_2-\tau_1)+g_{\mu\bar{\alpha}}(\tau_3-\tau_1)$$

$$-g_{\mu\nu}(\tau_3-\tau_1)+g_{\mu\nu}(\tau_4-\tau_1)-g_{\mu\bar{\alpha}}(\tau_3-\tau_2)$$

$$+g_{\mu\nu}(\tau_3-\tau_2)-g_{\mu\nu}(\tau_4-\tau_2)+g_{\bar{\alpha}\bar{\alpha}}(\tau_3-\tau_2)$$

$$-g_{\bar{\alpha}\nu}(\tau_3-\tau_2)+g_{\bar{\alpha}\nu}(\tau_4-\tau_2)-g_{\bar{\alpha}\nu}(\tau_4-\tau_3)$$

$$+g_{\nu\nu}(\tau_4-\tau_3). \tag{B7}$$

The line broadening functions $g_{\bar{mn}}(\tau)$ where Latin indices assume the values μ, $\bar{\mu}$, $\mu\nu$, and $\bar{\mu}\bar{\nu}$ are expressed in terms of spectral densities $C_{\bar{mn}}(\omega)$ using Eq. (7).

$R(t_3,\infty,t_1)$ in Eq. (B2) can be expressed in terms of the doorway and windows functions $D_\mu(t)$ and $W_\mu(t)$ which are calculated in Appendix C:

$$R(t_3,\infty,t_1)=\sum_\mu W_\mu(t_3)D_\mu(t_1)+W_0(t_3)D_0(t_1). \tag{B8}$$

Combining Eqs. (B2) and (B8) yields the first term in Eq. (16)

$$R^{(c)}(t_3,t_2,t_1)=R(t_3,t_2,t_1)-\sum_\mu W_\mu(t_3)D_\mu(t_1)$$

$$-W_0(t_3)D_0(t_1). \tag{B9}$$

APPENDIX C: THE SEQUENTIAL COMPONENT

In this Appendix we calculate the functions $D_\mu(t)$, $W_\mu(t)$, and $K_{\mu\nu}(t)$ introduced in Eq. (16). Using a perturbative expansion in H_1, we note that the leading contribution to $D_\mu(t)$ and $W_\mu(t)$ is the zeroth order. Equations (A16) and (A19) show that the expansion of $D_\nu^{(1)}(\tau,t)$ and $W_\mu^{(1)}(\tau,t)$ starts with first-order terms. Using our prescription of evaluating all quantities to lowest order in H_1, we can neglect the latter term and obtain

$$\bar{D}_\nu(\tau,t)=D_\nu(t)\delta(\tau),$$

$$\bar{W}_\mu(t,\tau)=W_\mu(t)\delta(\tau). \tag{C1}$$

Starting with Eqs. (A15), (A18), (A25) and (A26) D_ν, W_μ as well as D_0, and W_0 (in Eq. (9)) can be represented in a form

$$D_\nu(t)=D_\nu^L(t)+D_\nu^L(-t),$$

$$W_\mu(t)=W_\mu^L(t)-W_\mu^L(-t), \tag{C2}$$

with

$$D_\nu^L(t)\equiv-d_\nu^2\mathrm{Tr}[B_\nu(t)B_\nu^\dagger(0)\bar{\rho}_0], \tag{C3}$$

$$W_\mu^L(t)\equiv id_\mu^2\mathrm{Tr}[B_\mu^\dagger(0)B_\mu(t)\bar{\rho}_\mu]$$

$$-i\sum_{\bar{\nu}} d_{\mu,\bar{\nu}}^2\mathrm{Tr}[B_\mu^\dagger(t)Y_{\bar{\nu}}(t)Y_{\bar{\nu}}^\dagger(0)B_\mu(0)\bar{\rho}_\mu], \tag{C4}$$

and

$$D_0(t)=-\sum_\nu D_\nu(t).$$

$$W_0(t)=i\sum_\mu [D_\mu^L(t)-D_\mu^L(-t)]\}. \tag{C5}$$

The kernel $\bar{K}_{\mu\nu}(t)$ is calculated in second order in H_1, in this case Eq. (A22) yields

$$\bar{K}_{\mu\nu}(t)=K_{\mu\nu}^L(t)+K_{\mu\nu}^L(-t), \tag{C6}$$

with

$$K_{\mu\nu}^L(\tau)=\mathrm{Tr}[B_\nu^\dagger(\tau)B_\mu(\tau)q_{\nu\mu}^{(c)}(\tau)B_\mu^\dagger(0)B_\nu(0)$$

$$\times q_{\mu\nu}^{(c)}(0)\bar{\rho}_\nu], \tag{C7}$$

for $\tau>0$ and for $\tau<0$ we have

$$K_{\mu\nu}^L(\tau)=[K_{\mu\nu}^L(-\tau)]^*. \tag{C8}$$

Equation (C3) represents $D_\nu^L(t)$ in terms of a correlation function with respect to $\bar{\rho}_0$.

Equations (C4) and (C7) can be transformed to a similar form using the relation

$$\bar{\rho}_\mu=\lim_{t\to\infty} \exp(-iL_0t)B_\mu^\dagger\bar{\rho}_0B_\mu. \tag{C9}$$

Substituting Eq. (C9) into Eqs. (C4) and (C7) yields

$$W_\mu^L(\tau)=id_\mu^2\lim_{t\to\infty} \mathrm{Tr}[B_\mu(-t)B_\mu^\dagger(0)B_\mu(\tau)B_\mu^\dagger(-t)\bar{\rho}_0]$$

$$-\sum_{\bar{\nu}} id_{\mu,\bar{\nu}}^2\lim_{t\to\infty} \mathrm{Tr}[B_\mu(-t)B_\mu^\dagger(\tau)Y_{\bar{\nu}}(\tau)Y_{\bar{\nu}}^\dagger(0)$$

$$\times B_\mu(0)B_\mu^\dagger(-t)\bar{\rho}_0], \tag{C10}$$

$$K_{\mu\nu}^L(\tau)=\lim_{t\to\infty} \mathrm{Tr}[B_\nu(-t)B_\nu^\dagger(\tau)B_\mu(\tau)q_{\nu\mu}^{(c)}(\tau)B_\mu^\dagger(0)$$

$$\times B_\nu(0)q_{\mu\nu}^{(c)}(0)B_\nu^\dagger(-t)\bar{\rho}_0]. \tag{C11}$$

Equation (C9), used in the derivation of Eqs. (C10) and (C11), may be interpreted as follows: We start with the system in the ground electronic state, at thermal equilibrium with the density matrix $\bar{\rho}_0$, and excite the μth exciton. The system will reach equilibrium for the μth exciton, i.e. $\bar{\rho}_\mu$ after large enough time t. Formally the limit in the r.h.s. of Eq. (C9) does not exist since the full density matrix of a closed system does not equilibrate. However, this limit exists in a weak sense, i.e. we can use Eq. (C9) to calculate expectation values which are related to reduced variables which do equilibrate. This implies that the limits in Eqs. (C10) and (C11) do exist in the full sense.

The correlation functions in Eqs. (C3) and (C10), can be evaluated using the second order cumulant expansion (which is exact for this model) using the procedure described in Ref. 33. A straightforward calculation yields

$$D_\nu^L(t)=-d_\nu^2 \exp[-i\epsilon_\nu t-g_{\nu\nu}(t)], \tag{C12}$$

$$W_\mu^L(\tau) = \lim_{t\to\infty}\left\{ id_\mu^2 \exp[-f_{\mu\mu}^{(1)}(-t,0,\tau,-t)]\exp[-i\epsilon_\mu\tau]\right.$$

$$-\sum_{\bar\nu} id_{\mu,\bar\nu}^2 \exp[-f_{\mu\mu,\bar\nu}^{(2)}(-t,\tau,0,-t)]$$

$$\left.\times \exp[-i(\epsilon_{\bar\nu}-\epsilon_\mu)\tau]\right\}. \tag{C13}$$

Explicit expressions for $W_\mu^L(\tau)$ are obtained by substituting the following identities into Eq. (C13)

$$\lim_{t\to\infty} f_{\mu\mu}^{(1)}(-t,0,\tau,-t) = g_{\mu\mu}^*(\tau)-2i\lambda_{\mu\mu}\tau, \tag{C14}$$

$$\lim_{t\to\infty} f_{\mu\mu,\bar\nu}^{(2)}(-t,\tau,0,-t) = g_{\mu\mu}(\tau)+g_{\bar\nu\bar\nu}(\tau)-2g_{\mu\bar\nu}(\tau)$$

$$-2i(\lambda_{\mu\bar\nu}-\lambda_{\mu\mu})\tau. \tag{C15}$$

To evaluate $K_{\mu\nu}^L(\tau)$ we first represent Eq. (C11) in a form

$$K_{\mu\nu}^L(\tau) = \frac{\partial^2}{\partial\alpha\partial\beta}\lim_{t\to\infty} \mathrm{Tr}\{B_\nu(-t)B_\nu^\dagger(\tau)B_\mu(\tau)$$

$$\times \exp[i\alpha q_{\nu\mu}^{(c)}(\tau)]B_\mu^\dagger(0)B_\nu(0)$$

$$\times \exp[-i\beta q_{\mu\nu}^{(c)}(0)]B_\nu^\dagger(-t)\bar\rho_0\}|_{\alpha=\beta=0}. \tag{C16}$$

The correlation function in the r.h.s. of Eq. (C16) was evaluated using the second order cumulant. A similar calculation has been performed in Ref. 35 where the terms $\exp(i\alpha q)$ appeared due to non-Condon effects. A straightforward but tedious calculation yields

$$K_{\mu\nu}^L(\tau) = K_{\mu\nu}^F(\tau)\{\ddot g_{\mu\nu,\nu\mu}(\tau)-[\dot g_{\nu\mu,\nu\nu}(\tau)-\dot g_{\nu\mu,\mu\mu}(\tau)$$

$$+2i\lambda_{\nu\mu,\nu\nu}][\dot g_{\nu\nu,\mu\nu}(\tau)-\dot g_{\mu\mu,\mu\nu}(\tau)$$

$$+2i\lambda_{\mu\nu,\nu\nu}]\} \quad \text{for } \tau>0. \tag{C17}$$

Here dots stand for time derivative, and

$$K_{\mu\nu}^F(\tau) \equiv \exp[-i(\epsilon_\mu-\epsilon_\nu)\tau - g_{\mu\mu,\mu\mu}(\tau) - g_{\nu\nu,\nu\nu}(\tau)$$

$$+g_{\nu\nu,\mu\mu}(\tau)+g_{\mu\mu,\nu\nu}(\tau)-2i(\lambda_{\nu\nu,\nu\nu}-\lambda_{\mu\mu,\nu\nu})\tau], \tag{C18}$$

where we have used the notation

$$\lambda_{\mu\nu,\mu'\nu'} \equiv -\lim_{\tau\to\infty}\mathrm{Im}\left[\frac{dg_{\mu\nu,\mu'\nu'}(\tau)}{d\tau}\right]. \tag{C19}$$

The terms with $\dot g(\tau)$ and $\ddot g(\tau)$ in Eq. (C17) have the following origin. In the absence of the $\exp(i\alpha q)$ and $\exp(-i\beta q)$ terms, the second-order cumulant contains double time integrals of the collective coordinate correlation function which yields the line broadening functions $g(\tau)$.[23,34] The term in the second-order cumulant which originates from $q_{\nu\mu}^{(c)}(\tau)$ and $q_{\mu\nu}^{(c)}(0)$ has the form $\langle q_{\nu\mu}^{(c)}(\tau)q_{\mu\nu}^{(c)}(0)\rangle$ and is naturally represented by the second time derivative of the line broadening

function, $\ddot g(\tau)$. The mixed terms contain single time integrals of the coordinate correlation functions are represented by $\dot g(\tau)$.

APPENDIX D: FINAL EXPRESSIONS FOR THE RESPONSE FUNCTION; THE ROTATING WAVE APPROXIMATION

In this Appendix we summarize all quantities used in the numerical calculations of Eq. (16).

First we calculate $R^{(c)}$: Starting from Eq. (B9), for the pulse configuration of Eq. (19), only three out of 16 terms (see Eq. (B3)) contribute to $R(t_3,t_2,t_1)$ within the rotating wave approximation. The corresponding double-sided Feynman diagrams are given in Fig. 2.

$$R(t_3,t_2,t_1) = R_I(t_3,t_2,t_1)+R_{II}(t_3,t_2,t_1)$$

$$+R_{III}(t_3,t_2,t_1), \tag{D1}$$

$$R_I(t_3,t_2,t_1) = -i\sum_{\mu\nu} d_\mu d_\mu d_\nu d_\nu \exp[-f_{\mu\nu}^{(1)}(0,t_2+t_1,t_3$$

$$+t_2+t_1,t_1)]\exp[-i\epsilon_\mu(t_3+t_2)$$

$$+i\epsilon_\nu(t_2+t_1)], \tag{D2}$$

$$R_{II}(t_3,t_2,t_1) = -i\sum_{\mu\nu} d_\mu d_\mu d_\nu d_\nu \exp[-f_{\mu\nu}^{(1)}(0,t_1,t_3+t_2$$

$$+t_1,t_2+t_1)]\exp[-i\epsilon_\mu t_3+i\epsilon_\nu t_1], \tag{D3}$$

$$R_{III}(t_3,t_2,t_1) = -i\left\{ \sum_{\mu\nu\bar\alpha} d_{\mu\bar\alpha}d_{\nu\bar\alpha}d_\nu d_\mu \exp[-f_{\mu\nu,\bar\alpha}^{(2)}\right.$$

$$\times(t_1,t_2+t_1,t_3+t_2+t_1,0)]\exp[-i\epsilon_\mu(t_3$$

$$\left.+t_2+t_1)+i\epsilon_{\bar\nu}t_3+i\epsilon_\nu t_2]\right\}^*. \tag{D4}$$

In terms of Eq. (B3) we have $R_I=R_{21}$, $R_{II}=R_{31}$, and $R_{III}=-R_{12}^*$.

The other terms in Eq. (B9) are given by

$$\sum_\mu W_\mu(t_3)D_\mu(t_1)$$

$$= -i\sum_\mu d_\mu^2 \exp[i\epsilon_\mu t_1-g_{\mu\mu}^*(t_1)]\left\{ d_\mu^2 \exp[-i\epsilon_\mu t_3\right.$$

$$-g_{\mu\mu}^*(t_3)+2i\lambda_{\mu\mu}t_3] - \sum_{\bar\nu} d_{\mu,\bar\nu}^2$$

$$\times \exp[-i(\epsilon_{\bar\nu}-\epsilon_\mu)t_3-g_{\mu\mu}(t_3)-g_{\bar\nu\bar\nu}(t_3)+2g_{\mu\bar\nu}(t_3)$$

$$\left.+2i(\lambda_{\mu\bar\nu}-\lambda_{\mu\mu})t_3]\right\}, \tag{D5}$$

and

$$W_0(t_3)D_0(t_1) = -i\sum_{\mu\nu} d_\nu^2 d_\mu^2 \exp[i\epsilon_\nu t_1-g_{\nu\nu}^*(t_1)]$$

$$\times \exp[-i\epsilon_\mu t_3-g_{\mu\mu}(t_3)]. \tag{D6}$$

Combining these terms we finally have for the second term in Eq. (16): where Eq. (D6) also defines the bleaching, (see Eq. (16)).

$$\sum_{\mu\nu} W_{\mu}(t_3) G_{\mu\nu}(t_2) D_{\nu}(t_1)$$

$$= -i \sum_{\mu\nu} d_{\nu}^2 \exp[i\epsilon_{\nu}t_1 - g_{\nu\nu}^*(t_1)] G_{\mu\nu}(t_2)$$

$$\times \left\{ d_{\mu}^2 \exp[-i\epsilon_{\mu}t_3 - g_{\mu\mu}^*(t_3) + 2i\lambda_{\mu\mu}t_3] \right.$$

$$- \sum_{\bar{\nu}} d_{\mu,\bar{\nu}}^2 \exp[-i(\epsilon_{\bar{\nu}} - \epsilon_{\mu})t_3 - g_{\mu\mu}(t_3) - g_{\bar{\nu}\bar{\nu}}(t_3)$$

$$\left. + 2g_{\mu\bar{\nu}}(t_3) + 2i(\lambda_{\mu\bar{\nu}} - \lambda_{\mu\mu})t_3] \right\}, \tag{D7}$$

where $G_{\mu\nu}(t_2)$ is calculated numerically by solving Eq. (A23).

Finally, the bleaching contribution is given by Eq. (D6).

[1] R. van Grondelle, J. P. Dekker, T. Gillbro, and V. Sundström, Biochim. Biophys. Acta **1187**, 1 (1994).

[2] V. Sundström and R. van Grondelle, in *Anoxygenic Photosynthetic Bacteria*, edited by R. E. Blankenship, M. T. Madiga, and C. E. Baner, page 349 (Kluwer Academic, Dordrecht, 1995).

[3] J. Phys. Chem. B **101** (1997) (Special Issue on Light-Harvesting Physics Workshop).

[4] S. E. Bradforth, R. Jimenez, F. van Mourik, R. van Grondelle, and G. R. Fleming, J. Phys. Chem. **99**, 16179 (1995).

[5] R. Jimenez, S. N. Dikshit, S. E. Bradforth, and G. R. Fleming, J. Phys. Chem. **100**, 6825 (1996).

[6] H. van der Laan, T. Schmidt, R. W. Visschers,K. J. Visschers, R. van Grondelle, and S. Völker, Chem. Phys. Lett. **170**, 231 (1990).

[7] N. R. S. Reddy, G. J. Small, M. Seibert, and R. Picorel, Chem. Phys. Lett. **181**, 391 (1991).

[8] N. R. S. Reddy, R. J. Cogdell, L. Zhao, and G. J. Small, Photochem. Photobiol. **57**, 35 (1993).

[9] C. D. Caro, R. W. Visschers, R. van Grondelle, and S. Völker, J. Phys. Chem. **98**, 10584 (1994).

[10] T. Pullerits, M. Chachisvilis, and V. Sundström, J. Phys. Chem. **100**, 10787 (1996).

[11] T. Pullerits, M. Chachisvilis, M. R. Jones, C. N. Hunter, and V. Sundström, Chem. Phys. Lett. **224**, 355 (1994).

[12] V. Nagarajan, R. G. Alden, J. C. Williams, and W. W. Parson, Proc. Natl. Acad. Sci. USA **93**, 13774 (1996).

[13] M. Chachisvilis, ''*Electronic and vibrational coherence in photosynthetic and model systems,*'' PhD thesis, Lund University, 1996.

[14] S. De Silvestri, A. M. Weiner, J. G. Fujimoto, E. P. Ippen, Chem. Phys. Lett. **112**, 195 (1984); A. M. Weiner, S. De Silvestri, E. P. Ippen, J. Opt. Soc. Am. B **2**, 654 (1985); T. Joo, A. C. Albrecht, Chem. Phys. **176**, 233 (1993).

[15] (a) T. Joo, Y. W. Jia, J. Y. Yu, D. M. Jonas, and G. R. Fleming, J. Phys. Chem. **100**, 2399 (1996); (b) R. Jimenez, F. van Mourik, J. Y. Yu, and G. R. Fleming, J. Phys. Chem. B **101**, 7350 (1997); (c) J. Y. Yu, Y. Nagasawa, R. van Grondelle, and G. R. Fleming, Chem. Phys. Lett. **280**, 404 (1997).

[16] W. P. de Boeij, Ph.D. thesis, University of Groningen (1997).

[17] E. A. Silinsh and V. Čápek, *Organic Molecular Crystals* (American Institute of Physics, New York, 1994).

[18] M. Pope and C. E. Swenberg, *Electronic Processes in Organic Crystals* (Clarendon Press, New York, 1982).

[19] V. Chernyak and S. Mukamel, in *Notions and Perspectives of Nonlinear Optics*, edited by O. Keller (World Scientific, Singapore, 1996), p. 93.

[20] (a) T. Meier, V. Chernyak, and S. Mukamel, J. Phys. Chem. B **101**, 7332 (1997); (b) T. Meier, Y. Zhao, V. Chernyak, and S. Mukamel, J. Chem. Phys. **107**, 3876 (1997).

[21] (a) T. Meier, V. Chernyak, and S. Mukamel, J. Chem. Phys. **107**, 8759 (1997); (b) W. M. Zhang, T. Meier, V. Chernyak, and S. Mukamel, Philos. Trans. R. Soc. London, Ser. A **356**, 405 (1998).

[22] R. A. Marcus and N. Sutin, Biochim. Biophys. Acta **811**, 265 (1985).

[23] S. Mukamel, *Principles of Nonlinear Optical Spectroscopy* (Oxford University Press, New York, 1995).

[24] In Ref. 21 we used the same symbols to denote the operators in real space (B_n) and in the exciton representation B_{μ}. For clarity, in this article we label the real space operators with an overbar. Note that we use the convention of Ref. 23 for Feynman diagrams (Fig. 2), which is different from that of Ref. 21(a). Apart from these changes, we use the same notation as in Ref. 21(a).

[25] M. Lindberg, R. Binder, and S. W. Koch, Phys. Rev. A **45**, 1865 (1992).

[26] T. Meier, S. Tretiak, V. Chernyak, and S. Mukamel, Phys. Rev. B **55**, 4960 (1997).

[27] K. Sauer, R. J. Cogdell, S. M. Prince, A. Freer, N. W. Isaacs, and H. Scheer, Photochem. Photobiol. **64**, 564 (1996).

[28] G. McDermott, S. M. Prince, A. A. Freer, A. M. Hawthornthwaite-Lawless, M. Z. Papiz, R. J. Cogdell, and N. W. Isaacs, Nature (London) **374**, 517 (1995).

[29] H. Tacker, Rev. Mod. Phys. **53**, 253 (1981); R. Baxter, *Exactly Solvable Models in Statistical Mechanics* (Academic, London, 1982).

[30] L. Allen and J. H. Eberly, *Optical Resonances and Two-Level Atoms* (Wiley, New York, 1975).

[31] H. Haug and S. W. Koch, *Quantum Theory of the Optical and Electronic Properties of Semiconductors* (World Scientific, Singapore, 1994).

[32] R. Zwanzig, Lect. Theor. Phys. **3**, 106 (1961); Physica (Utrecht) **30**, 1109 (1964).

[33] S. Mukamel and R. E. Smalley, J. Chem. Phys. **73**, 4156 (1980).

[34] S. Mukamel, Phys. Rev. A **28**, 3480 (1983).

[35] V. Khidekel, V. Chernyak, and S. Mukamel, J. Chem. Phys. **105**, 8543 (1996); V. M. Axt and S. Mukamel, Rev. Mod. Phys. **70**, 145 (1998).